www.sciencemag.org/cgi/content/full/science.aad7969/DC1

Supplementary Materials for

Pulmonary neuroendocrine cells function as airway sensors to control lung immune response

Kelsey Branchfield, Leah Nantie, Jamie M. Verheyden,
Pengfei Sui, Mark D. Wienhold, Xin Sun*

*Corresponding author. E-mail: xsun@wisc.edu

Published 7 January 2016 on *Science* First Release
DOI: 10.1126/science.aad7969

This PDF file includes:

Materials and Methods

Animals and tissues

Since *Robo1* and *Robo2* genes are both on chromosome 16, separated only by approximately 1.1 centimorgans, we bred mice carrying *Robo1* and *Robo2* mutant alleles in *cis* as previously described(*16, 25*). For conditional mutants, mice that were heterozygous for $Robo1^{-}$ mutant allele and $Robo2^{fl}$ were mated to mice carrying either a Shh^{cre} *or Ascl1creERT2* allele(*15, 17*). Induction of *Ascl1creERT2* activity was achieved through intraperitoneal injections of tamoxifen (25 mg/kg/day) and progesterone (18.75 mg/kg/day) (Sigma-Aldrich) dissolved in canola oil. For Robo-LacZ analyses, heterozygotes for *Robo1* and *Robo2* mutant alleles, which carry *lacZ* reporter insertions, were used(*16*). *Cgrp*, *Slit1*, *Slit2* and *Slit3* mutant alleles and GAD1-GFP (Gad67-GFP) transgene have been previously described(*20, 26-28*). Mutants were bred in mixed genetic background and littermate cre heterozygotes were used as control. Postnatal lungs were perfused with ice cold PBS to remove blood and then gravity inflated to a pressure of 20cm H20 with 4% paraformaldehyde. Following fixation, lungs were embedded for either paraffin, frozen or vibratome sectioning.

Expression pattern analyses

Immunofluorescent staining was performed on sections using a standard protocols. For immunohistochemical staining, a DAB kit (Vector Laboratories) was used for antigen detection. The following primary antibodies were used: rabbit anti-CGRP [1:200] (Sigma), mouse anti-CGRP [1:200] (Abcam), mouse anti-acetylated tubulin [1:200] (Sigma), rat anti-PECAM [1:100] (BD Biosciences), mouse anti-Ascl1 (MASH1)[1:100] (BD Biosciences), rabbit anti-synaptophysin [1:100] (NeoMarkers), rabbit anti-CD45 [1:200] (US Biological), mouse anti-smooth muscle alpha-actin Cy3 conjugated [1:500] (Sigma), rabbit anti-cleaved Caspase 3 [1:100] (Cell Signaling Technology), rat anti-Ly-6B.2 Allogantigen [1:100](AbD Serotec), rabbit anti-SPC [1:200] (Seven Hills Bioreagents), Syrian hamster anti-T1alpha (podoplanin) [1:200] (Developmental Studies Hybridoma Bank), rabbit anti-CD3 [1:200] (Abcam), goat anti-EMBP [1:100] (Santa Cruz Biotechnology), goat anti-Arginase [1:50] (Santa Cruz Biotechnology), rabbit anti-iNOS [1:100] (Abcam), rat anti-F4/80 [1400] (Abcam), rat anti-endomucin [1:100] (eBiosciences), rabbit anti-Hopx [1:100] (Santa Cruz Biotechnology), rabbit anti-tropelastin [1:100] (Abcam) and Isolectin B4-FITC [1:200] (Sigma-Aldrich). The following secondary antibodies used were used: goat anti-rabbit Cy3, goat anti-rabbit HRP, goat anti-mouse HRP, goat anti-rat HRP, goat anti-rabbit FITC [1:400] (Jackson Immunoresearch).

For β-galactosidase (β-gal) staining, lungs were fixed in 4% paraformaldehyde with gluteraldehyde for 30 minutes. Fixed tissues were washed and stained with X-gal solution, and then cryosectioned before immunostaining.

RNA *in situ* hybridization was performed according to a standard protocol using previously described probes(*16*).

Quantitative RT-PCR (qRT-PCR) and gene expression microarray

Lungs from a minimum of 3 animals per genotype were separately homogenized in Trizol and RNA was extracted using an RNeasy Plus Mini Kit (Qiagen). cDNA was prepared with Superscript-III First-Strand Synthesis System (Invitrogen) and PCR quantified using SYBRgreen (Applied Biosystems). Three technical and three biological replicates were performed. mRNA levels were normalized to *β-actin* mRNA levels and compared using a Student's t-test. Results are reported as mRNA quantity relative to control ± SEM and considered statistically significant if $p \leq 0.05$. Primers used are below:

Robo2	5'-TTGGAGCAAGTTCACGGGAG-3' 5'-TAAGCCGCTCTGTTAGTCGG-3'
β-actin	5' - CGGCCAGGTCATCACTATTGGCAAC - 3′ 5' - GCCACAGGATTCCATACCCAAGAAG - 3′
Ascl1	5' - TCTGGCAAGATGGAGAGTGGAGC - 3′ 5' - AAAGAAGCAGGCTGCGGGAG - 3′
Synaptophysin	5' - CGCCAGACAGGAAACACATGC - 3′ 5' - CAGAGCACCAGGTTCAGGAAGC - 3′
Calbindin	5' - CTGCTCTTTCGATGCCAGCAAC - 3′ 5' - GTTTCGATGAAGCCGCTGTGG - 3′
Cholecystokinin	5' - CAAAGCTCCTTCTGGCCGCATGTC - 3′ 5' - ATCCATCCAGCCCATGTAGTCC - 3′
Gastrin releasing peptide	5' - ACGGTCCTGGCTAAGATGTATCC - 3′ 5' - TTCAGGCCGTCTCTGTCAGC - 3′
Substance P	5' - GGTCCGACAGTGACCAGATCAAG - 3′ 5' - AAAGAACTGCTGAGGCTTGGGTC - 3′
Chromogranin A	5' - TTCCCACTTCCATGCAGGCTAC - 3′ 5' - GCCTCTGTCTTTCCATCTCCATCC - 3′
Somatostatin	5' - TGCCACCGGGAAACAGGAAC - 3′ 5' - GGGCATCATTCTCTGTCTGGTTGG - 3′
Leu-enkephalin	5' - ATGGAGCCAGAAGAAGAAGCGAAC - 3′ 5' - AAGGTGTCTCCCTCATCTGCATC - 3′
Peptide YY	5' - TCCAAACTGCTCTTCACAGACGAC - 3′ 5' - TCACCACTGGTCCAAACCTTCTG - 3′
Calcitonin gene-related peptide	5' - CCTTTCCTGGTTGTCAGCATCTTG - 3′ 5' - CTGGGCTGCTTTCCAAGATTGAC - 3′
Endothelin 1	5' - GCTGGTGGAAGGAAGGAAACTACG - 3′ 5' - TCGGTTGTGCGTCAACTTCTGG - 3′
Ccl3	5' - CCTACAGCCGGAAGATTCCACG - 3′ 5' - ATCTGCCGGTTTCTCTTAGTCAGG - 3′
Cxcl2	5' - ACCAACCACCAGGCTACAGG - 3′

	5’ - GTTCTTGAAGTCAACCCTTGGCAG - 3′
Saa3	5’ - ACTATGATGCTGCCCGGAGG - 3′ 5’ - TCCCGTGAACTTCTGAACAGCCTC - 3′
Tnfα	5’ - CCACCACGCTCTTCTGTCTACTG - 3′ 5’ - GGCCATAGAACTGATGAGAGGGAG - 3′

For microarray, 3 *Shhcre;Robo1;2* mutant or 3 control lungs were pooled to capture biological variation. One microgram of RNA was submitted to the UW Gene Expression Center for RNA labeling and hybridization to a Mouse Gene 1.0 Array (Affymetrix). Differential gene expression and gene ontology analyses were performed using GeneSifter software (Geospiza).

Boyden chamber assay

GAD1-GFP positive PNECs were sorted from E15.5 GAD1-GFP/+ lungs. Briefly, 17 lungs were dissected and dissociated in a solution of 1 mg/mL collagenase/dispase (Roche) in PBS to obtain single cell suspension. Cell sorting was performed with a SORP BD FACSAria II (BD Biosciences) at the UW Carbone Cancer Center Flow Cytometry Laboratory. Boyden chamber assay for cell migration was performed as previously described(*16*). Briefly, sorted PNECs were suspended in RPMI 1640 Medium GlutaMAX (Life Technologies) and equal numbers of cells were seeded into the top chambers of a cell culture insert with 8 μm pore (BD Biosciences) coated on both sides with fibronectin (Sigma). Recombinant human Slit2-N protein [100 ng/mL] (PeproTech) or PBS was added to RPMI media and applied either to the top chamber for the first experiment or to the bottom chamber for the second experiment. Seeded chambers were incubated at 37°C for 9 hours and then fixed for 30 minutes in 4% paraformaldehyde. The top of the insert was wiped clean to remove cells that did not migrate. The insert was mounted in Vectashield with DAPI (Vector Laboratories) and migrated cells on the bottom of the insert were imaged. Nine non-overlapping field of view (5X) were imaged, which covered most of the insert surface. Each experiment was repeated five times. Results are reported as the mean relative ratio of migrated cells in the Slit media chamber divided by migrated cells in the control chamber. The ratios were subjected to a one sample t-test and considered statistically significant if $p \leq 0.05$.

Clodronate treatment

For depletion of macrophages, mice were treated with Clophosome®-A-Clodronate Liposomes, which contains clodronate encapsulated in liposomes, or control liposomes (FormuMax). Mice received intraperitoneal injections of clodronate liposomes or control liposomes (10 uL liposomes/g body weight) starting at P5, and subsequently once per week until dissection.

Quantifications of mean linear intercept and cell numbers

For mean linear intercept (MLI) quantification, the lungs of 4 animals per genotype and/or condition were compared. Images were collected using a 20X objective for 7 random tissue sections per lung. A grid with 14 lines of finite length (450 um) was placed

over each image and the number of intercepts was counted as the number of times an alveolar wall intersected the grid lines. The area covered by the grid lines was divided by the number of intercepts to give an MLI value. Thus a larger MLI value represents fewer intercepts and more simplified alveoli. Results are reported as mean MLI ± SEM and considered statistically significant if $p \leq 0.05$.

For cell quantifications (solitary PNECs, CD45+ immune cells, neutrophils, eosinophils, macrophages, T cells), 10 random sections were imaged using a 40X objective for the lungs of 3-4 animals per genotype and/or condition. For M1 and M2 macrophage identification, the number of iNOS and F4/80 double positive or arginase and F4/80 double positive cells were quantified as a percentage of total F4/80 positive macrophages. Results are reported as the mean or relative mean (normalized to control) ± SEM and considered statistically significant if $p \leq 0.05$.

For quantification of PNEC number in NEBs, thick (~100um) vibratome sections were prepared. Confocal z-stack images were collected through the cluster with 40X magnification and a z-step of 1um. Only clusters that were not touching either cut surface were counted to avoid clusters with cells cut off. DAPI staining and Synaptophysin staining in both 3D reconstruction and individual z-slices were used to accurately count each cell.

Supplementary Text

Extended technical descriptions of results

For Figure 1, qRT data displayed in 1C: *Ccl3* 3.47 ± 0.77 vs 1 ± 0.03, p = 0.03; *Cxcl2* 4.54 ± 0.74 vs 1 ± 0.22, p = 0.01; *Tnfa* 2.52 ± 0.58 vs 1 ± 0.35, $p = 4.98 \times 10^{-4}$; *Saa3* 18.63 ± 5.49 vs 1 ± 0.26, p = 0.03; n = 3 for each. Scale bars: (A,B) 200 μm, (D,E) 50 μm, (F) 100 μm, (G) 20 μm.

For Figure 3, qRT data displayed in 3A: Levels of the following are increased in *Shhcre;Robo* mutants compared to controls: *SubP* 1.48 ± 0.15 vs 1 ± 0.14, p = 0.02; *ChgA* 2.79 ± 0.63 vs 1 ± 0.34, p = 0.01; *Enk* 1.29 ± 0.11 vs 1 ± 0.07, p = 0.02; *Cgrp* 4.90 ± 0.68 vs 1 ± 0.96, $p = 4.65 \times 10^{-3}$; *Edn1* 2.20 ± 0.10 vs 1 ± 0.34, $p = 9.87 \times 10^{-4}$; n = 3 for each. * $p < 0.05$, ** $p < 0.001$. Quantification displayed in 3F, quantification presented as the relative percentage of macrophage to total cell ratio normalized to $Shhcre;Robo^{+/-};Cgrp^{+/+}$: $Shhcre;Robo^{-/-};Cgrp^{+/+}$ (2.80 ± 0.12) vs $Shhcre;Robo^{-/-};Cgrp^{+/-}$ (2.32 ± 0.08), p = 0.0097; *Shhcre;Robo* mutant; $Cgrp^{+/+}$ (2.80 ± 0.12) vs *Shhcre;Robo* mutant; $Cgrp^{-/-}$ (1.84 ± 0.18), $p = 1.26 \times 10^{-6}$; n = 4 each.

For Figure 4, macrophage quantification as the relative percentage of macrophage to total cell ratio normalized to control mice with liposome control treatment: *Shhcre;Robo* mutant with control treatment (2.80±0.14) compared to *Shhcre;Robo* mutant with clodronate treatment (1.17±0.12), $p = 9.4 \times 10^{-13}$; no significant difference between clodronate-treated *Shhcre;Robo* mutants and controls (1.17±0.07), p = 0.94, n = 4 each. For Figure 4J, quantification of mean linear intercept (MLI): clodronate-treated *Shhcre;Robo* mutant (36.14 ± 0.72) showed reduced MLI compared to control-treated *Shhcre;Robo* mutant (49.61um ± 1.22), $p = 2.5 \times 10^{-13}$, no significant difference between clodronate-treated *Shhcre;Robo* mutants and controls (35.15 ± 0.39), p = 0.14, n = 4 each.

Branchfield et al.
Figure S1

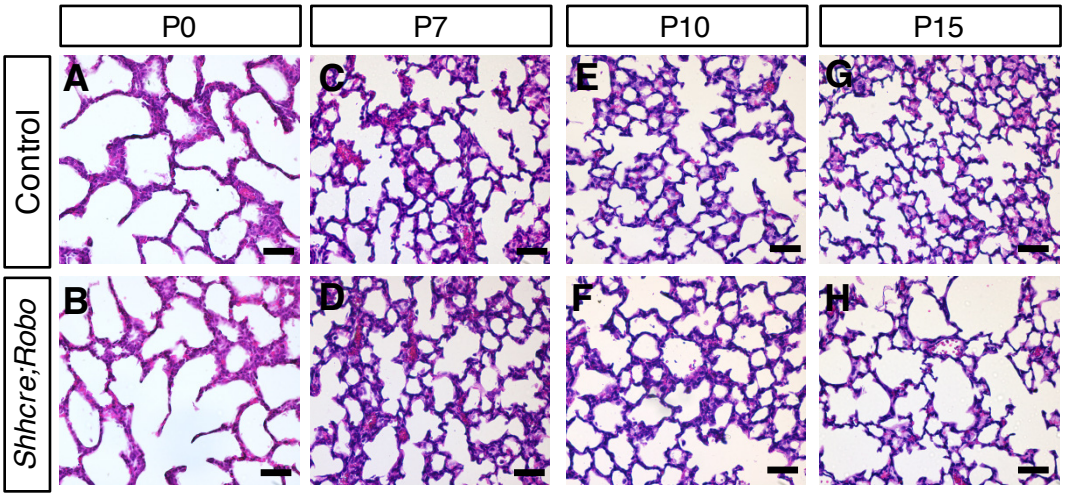

Figure S1. *Shhcre;Robo* mutants exhibit alveolar simplification starting at P15.
(A-H) H&E staining of paraffin sectioned alveolar regions of the lung of indicated genotypes at indicated stages.

Branchfield et al.
Figure S2

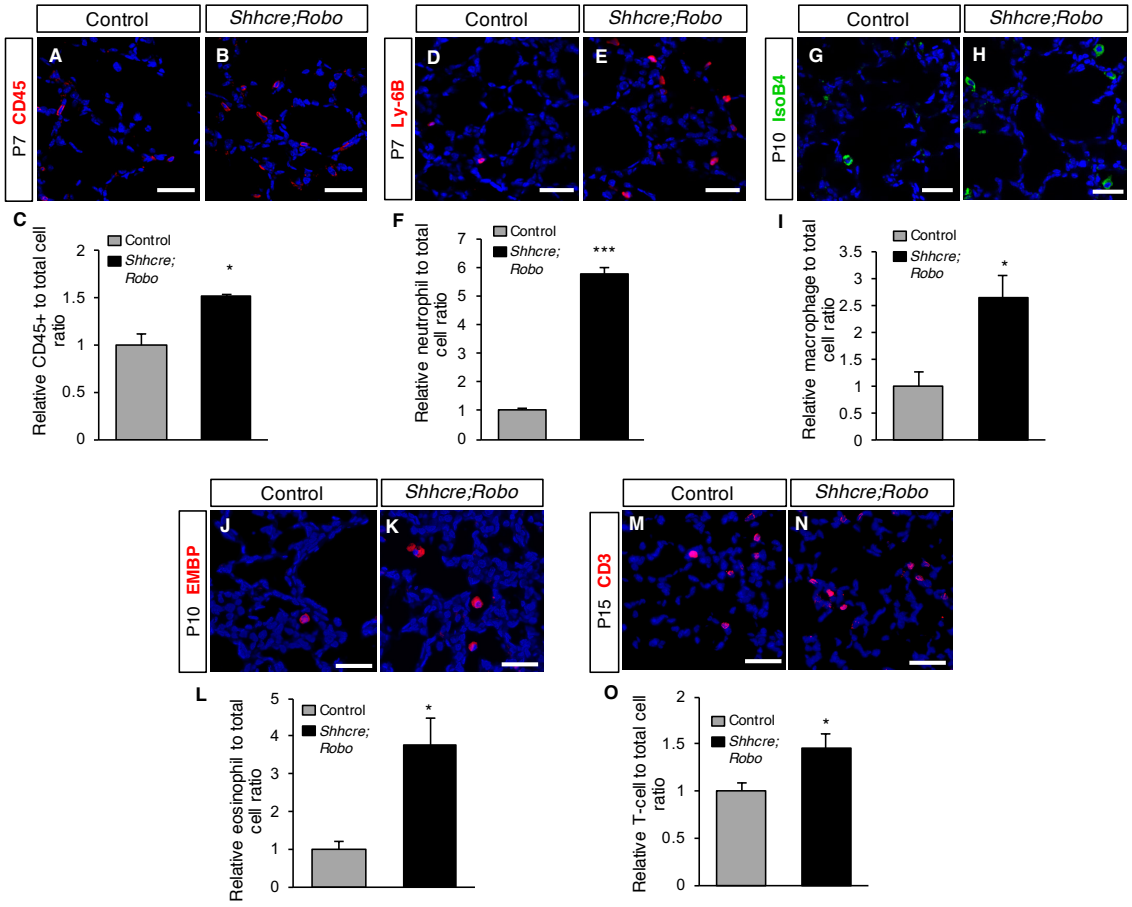

Figure S2. Immune infiltrates are increased prior to alveolar simplification in *Shhcre;Robo* mutant lungs.

(A,B) CD45 (leukocyte common antigen) immunostaining labels immune infiltrates in lungs at P7. (C) $CD45^{+}$ immune cells are increased in the mutant (1.51 ± 0.13) compared to control (1 ± 0.12) at P7, p = 0.015, n = 6 each. (D,E) Ly-6B immunostaining labels neutrophils in lungs at P7. (F) Neutrophils are increased in the mutant (5.76 ± 0.24) compared to the control (1 ± 0.08) at P7, $p = 1.96x10^{-32}$, n = 4 each. (G,H) IsoB4 immunostaining labels alveolar macrophages in lungs at P10. (**I**) Macrophages are increased in the mutant (2.66 ± 0.40) compared to the control (1 ± 0.29) at P10, p=0.007. (J,K) EMBP immunostaining labels eosinophils in lungs at P10. (**L**) Eosinophils are increased in the mutant (3.78 ± 0.72) compared to the control (1 ± 0.19) at P15, p=0.021. (M,N**)** CD3 immunostaining labels T-cells in lungs at p15. (O) T-cells are increased in the mutant (1.45 ± 0.16) compared to the control (1 ± 0.08) at P15, p=0.0413. n = 6 each (A-I) and n=3-4 each (J-O). *p<0.05, ***p<0.0001. Scale bars, 40 µm.

Branchfield et al.
Figure S3

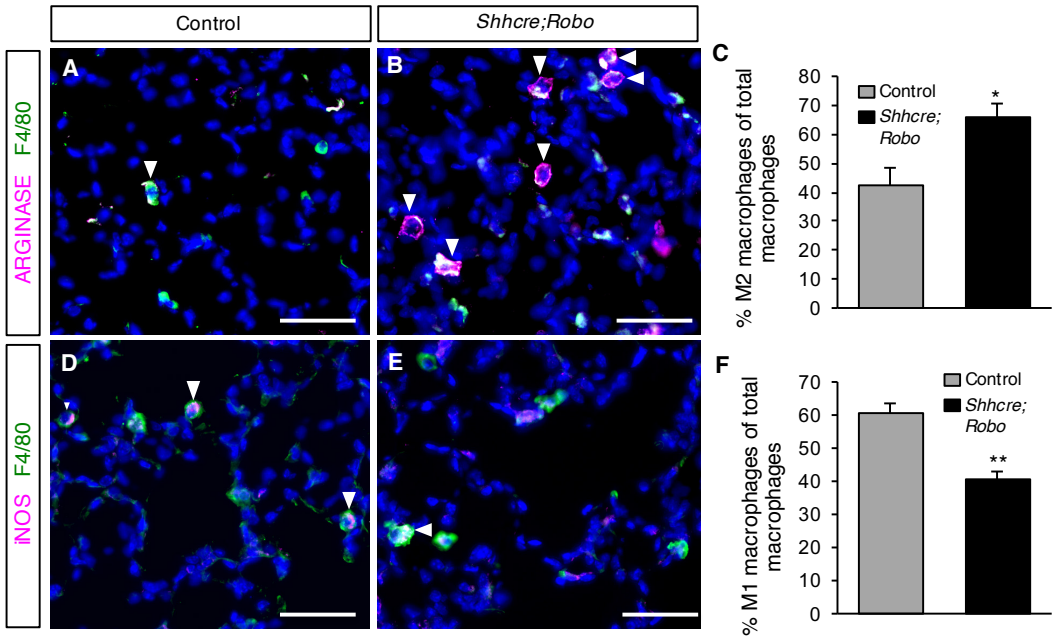

Figure S3. Percentage of M2 macrophages are increased in *Shhcre;Robo* mutant lungs.

(A,B) Arginase and F4/80 double positive immunostaining labels M2 (alternatively activated) macrophages in lungs at P22. (C) The percent of Arginase-positive macrophages among all macrophages (F4/80 immunostained cells) is increased in the mutant (65.63% ± 4.75) compared to control (42.24% ± 5.96) at P22, $p = 0.037$, $n = 3$ each. (D,E) iNOS and F4/80 double positive immunostaining labels M1 (classically activated) macrophages in lungs at P22. (F) The percent of iNOS-positive macrophages among all macrophages (F4/80 immunostained cells) is decreased in the mutant (40.72% ± 2.59) compared to control (60.82% ± 2.55) at P22, $p = 0.0052$, $n = 3$ each. *$p<0.05$, **$p<0.01$. Scale bars, 50 µm.

Branchfield et al.
Figure S4

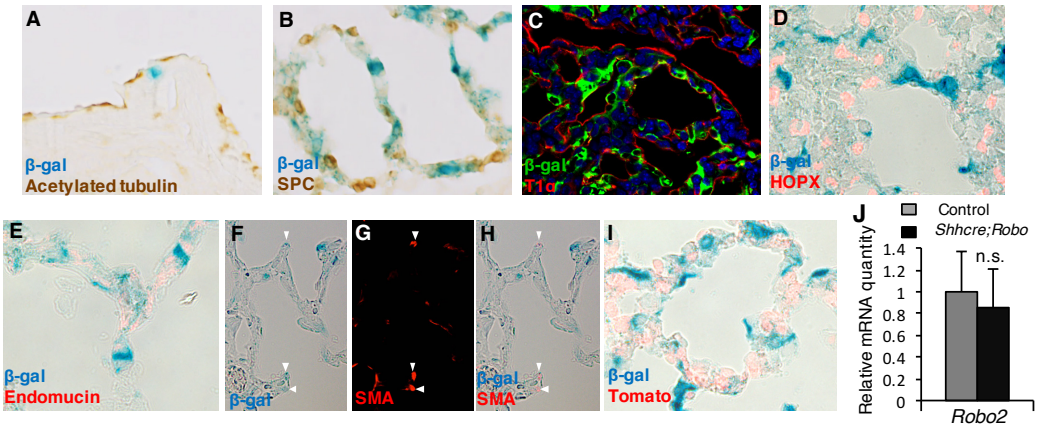

Figure S4. *Robo1;2* expression pattern with respect to epithelium and mesenchyme.

X-gal (A,B, E, F, H, I) or anti-β-gal immunofluorescent staining (C) on P0 or P7 (F-I) double heterozygous lungs expressing *lacZ* from *Robo1* and *Robo2* loci. Scale bars, 40 μm. (A) *Robo-LacZ* expression in the airway epithelium does not overlap with acetylated tubulin immunostaining of ciliated cells at P0. (B) *Robo-LacZ* expression in the alveolar region does not overlap with SPC immunostaining of type II cells at P0. (C) *Robo-LacZ* expression in the alveolar region does not overlap with T1α immunostaining of type I cells at P0. (D). *Robo-LacZ* expression does not overlap with HOPX staining of type I cells in the alveolar region at P0. (E) *Robo-LacZ* expression does not overlap with Endomucin immunostaining of blood vessels in the alveolar region at P0. (F,G,H) Some cells with *Robo-LacZ* expression overlap with SMA immunostaining in the alveolar region at P7, as indicated by arrowheads. (I) *Robo-LacZ* expression does not overlap with *Shhcre;tdTom* reporter expression in the alveolar region at P0. (J) *Robo2* level is not changed in the peripheral alveolar region of *Shhcre;Robo* mutant lungs as compared to control lungs at P26, n=3 each. n.s. = not significantly different p=0.651, Control=1±0.379 mutant=0.857± 0.352.

Branchfield et al.
Figure S5

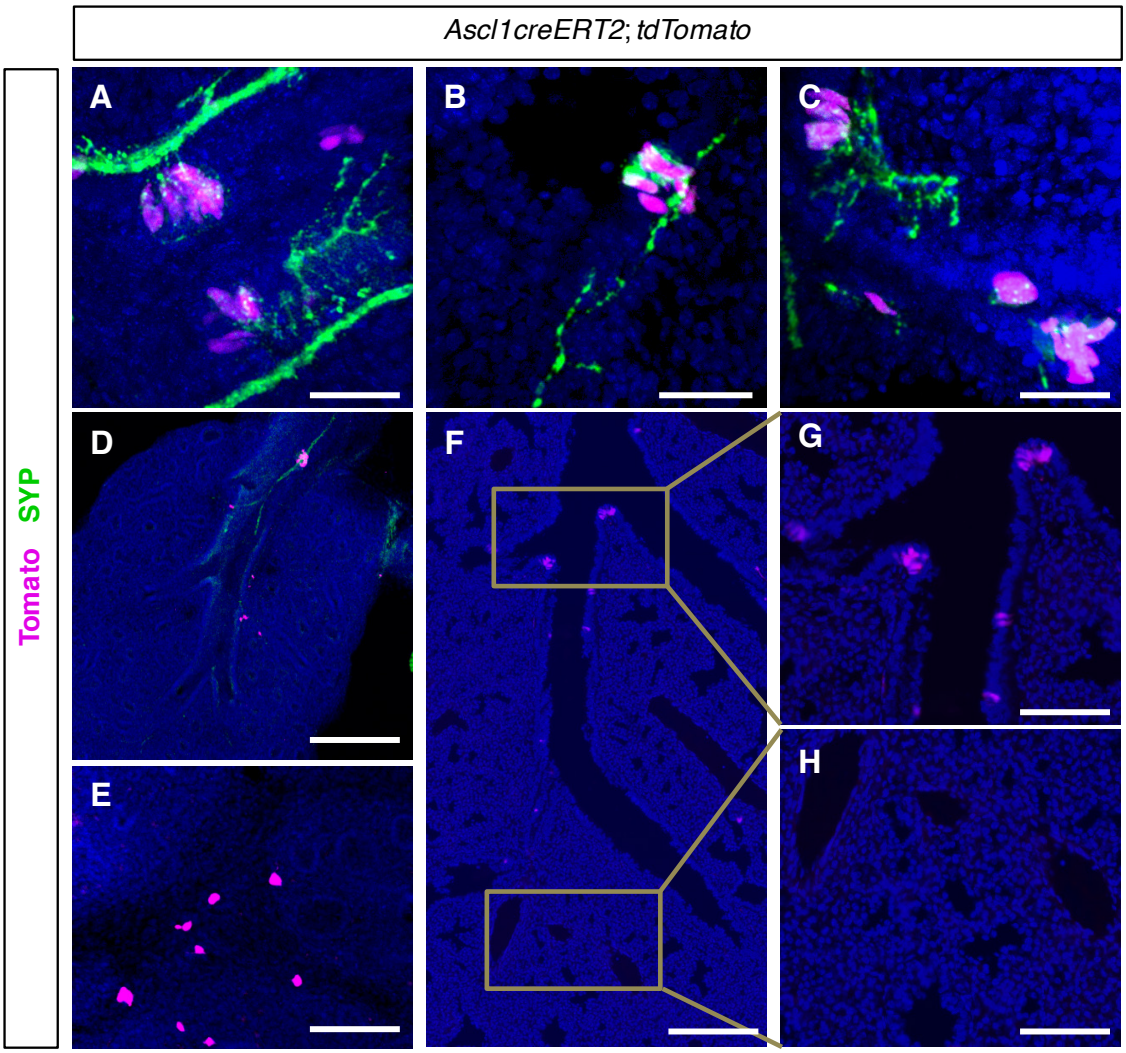

Figure S5. *Ascl1creERT2* activity.

(A-C) E15.5 lungs showing tdTomato reporter expression (magenta) driven by *AsclcreERT2* in PNECs (synaptophysin immunostaining, green). Tamoxifen induction was carried out at E13.5. Of 851 PNECs counted, 829 (97.4%) exhibited tdTomato reporter expression. Scale bars, 40 µm. (D,E) E15.5 lungs with tamoxifen induction at E12.5. (F-H) E18.5 lungs with tamoxifen induction at E16.5. No reporter activity is observed in the alveolar region. Scale bars in D and F are 400µm, in E,G and H are 200µm.

Branchfield et al.
Figure S6

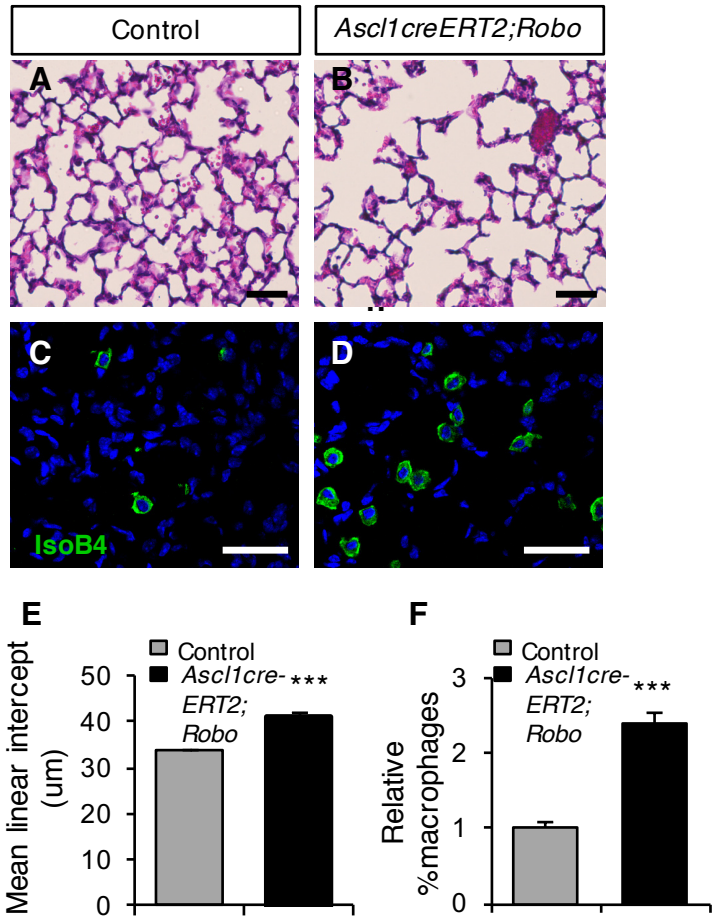

Figure S6. Inactivating *Robo* in PNECs using *Ascl1creERT2* recapitulate *Shhcre;Robo* phenotypes.

(A,B,E) Mean linear intercept is significantly increased, indicating a reduction in alveoli, in *Ascl1creERT2;Robo* lungs compared to controls: 41.29 μm ± 0.76 vs 33.69 μm ± 0.35, $p = 2.58 \times 10^{-11}$, n = 4. (C,D,F) Alveolar macrophages, quantified as normalized macrophage to total cell ratio, are significantly increased in *Ascl1creERT2;Robo* mutant lungs compared to controls: 2.41±0.11 vs 1±0.07, $p = 4.46 \times 10^{-18}$, n = 4 each. *** $p < 0.0001$.

Branchfield et al.
Figure S7

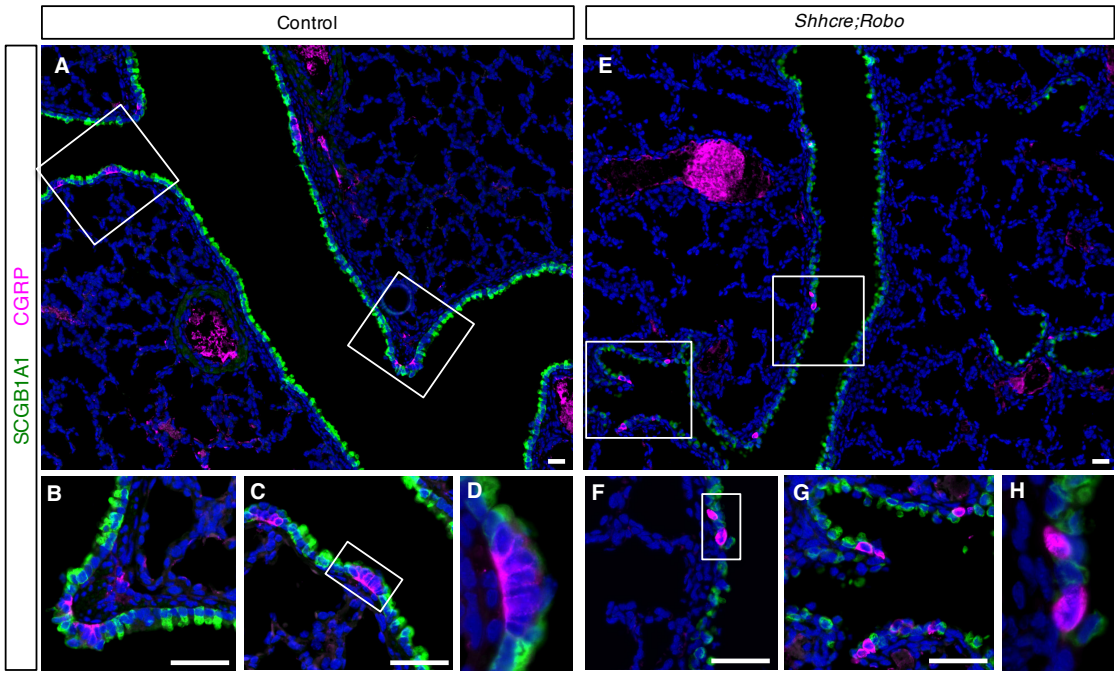

Figure S7. PNEC localization in the airway of control and *Shhcre;Robo* mutants.

(A-H) P4 lungs stained with anti-SCGB1A1 to label club cells and anti-CGRP to label PNECs. (A-D) PNECs are clustered into NEBs in the control lung. (E-H) PNECs are unclustered in the p4 *Shhcre;Robo* mutant lung. Boxes (A,C,E,F) indicate location of higher magnification photos (B-D, F-H), respectively. Scale bars, 50µm.

Branchfield et al.
Figure S8

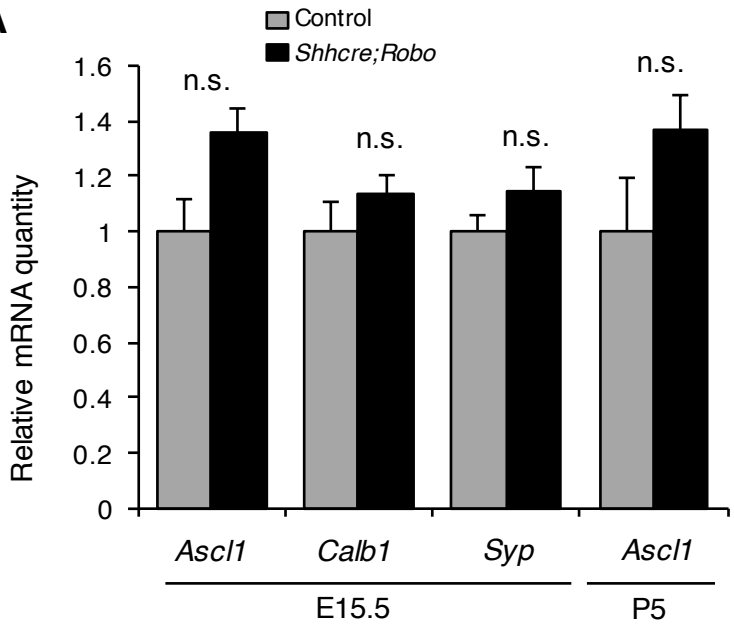

Figure S8. PNEC marker expression is not altered in *Shhcre;Robo* mutants.

(A) qRT-PCR analysis of transcript level of genes involved in PNEC specification (*Ascl1*) and structural components of PNECs (*Calb1* and *Syp*) in either E15.5 or P5 lungs. Transcript levels are not significantly different between mutant and control lungs (*Shhcre;Robo* mutant vs control: *Ascl1* [E15.5] 1.35 ± 0.09 vs 1 ± 0.11, p = 0.07; *Calb1* [15.5] 1.14 ± 0.06 vs 1 ± 0.11, p = 0.35; *Syp* [E15.5] 1.15 ± 0.09 vs 1 ± 0.06, p = 0.25; *Ascl1* [P5] 1.36 ± 0.13 vs 1 ± 0.19, p = 0.19). *Ascl1* = achaete-scute complex homolog 1, *Calb1* = calbindin 1, *Syp* = synaptophysin, n.s. = not significantly different, $p \geq 0.05$.

Branchfield et al.
Figure S9

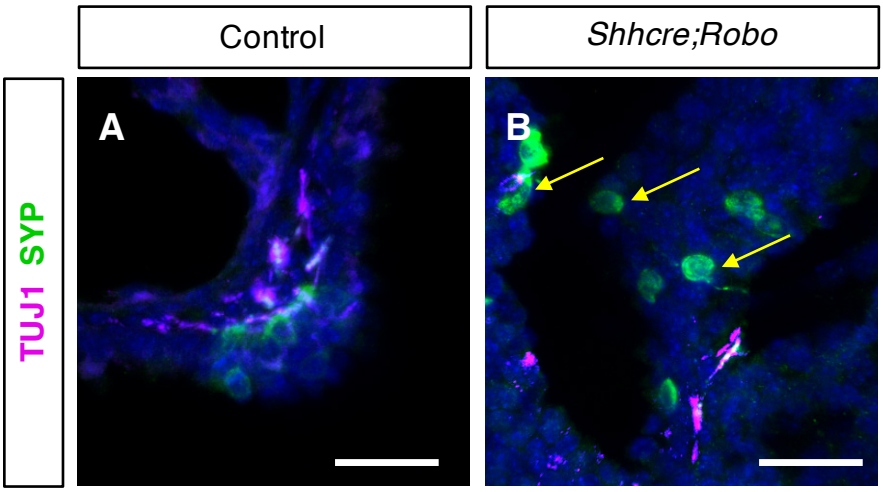

Figure S9. CGRP localization is altered in the *Shhcre;Robo* mutant.

(A,B) Confocal stack of vibratome airway sections stained with anti-TUJ1 to label nerves and CGRP to label PNEC and sensory nerve. In the control, an NEB is shown, and CGRP staining is polarized to the basal side of PNECs. In the mutant, solitary cells show increased intensity of CGRP staining and the signal is no longer polarized. In the control, the NEB is innervated. In the mutant, a subset of the solitary PNECs are innervated. Scale bars, 75 μm.

Branchfield et al.
Figure S10

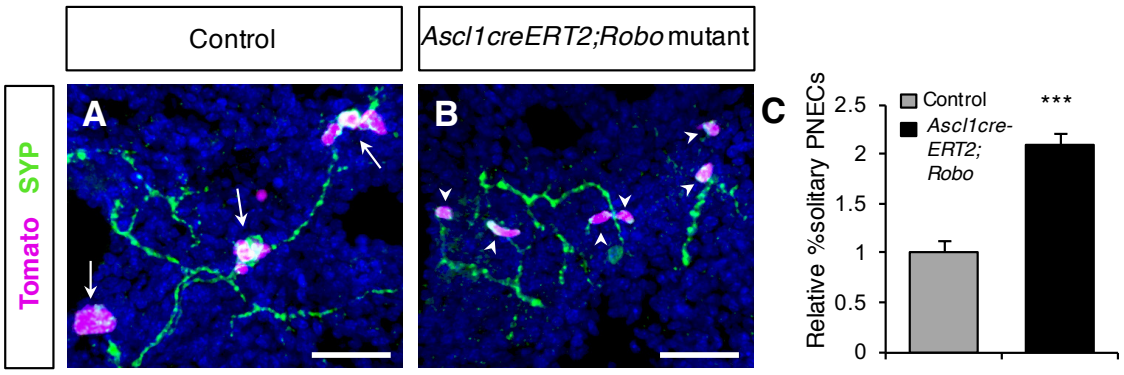

Figure S10. *Robo1;2* are required specifically in PNECs for NEB formation in *Ascl1creERT2;Robo* mutants.

(A,B) tdTomato cre reporter activity (magenta) labels PNECs where *Ascl1creERT2* has been induced in both the control and mutant. In the control, the labeled cells are in clusters (arrow), while in the mutant, they are solitary (arrowheads). P5 lung, with cre induced by tamoxifen at P0, synaptophysin immunostaining (green) labels PNECs and innervating nerves. Scale bars, 40 µm. (C) The relative percent of solitary (unclustered) PNECs is significantly increased in *Ascl1creERT2;Robo* mutants compared to controls: 2.10% ± 0.10 vs 1% ± 0.12, $p = 9.15 \times 10^{-5}$, n = 4 each. *** $p < 0.0001$.

Branchfield et al.
Figure S11

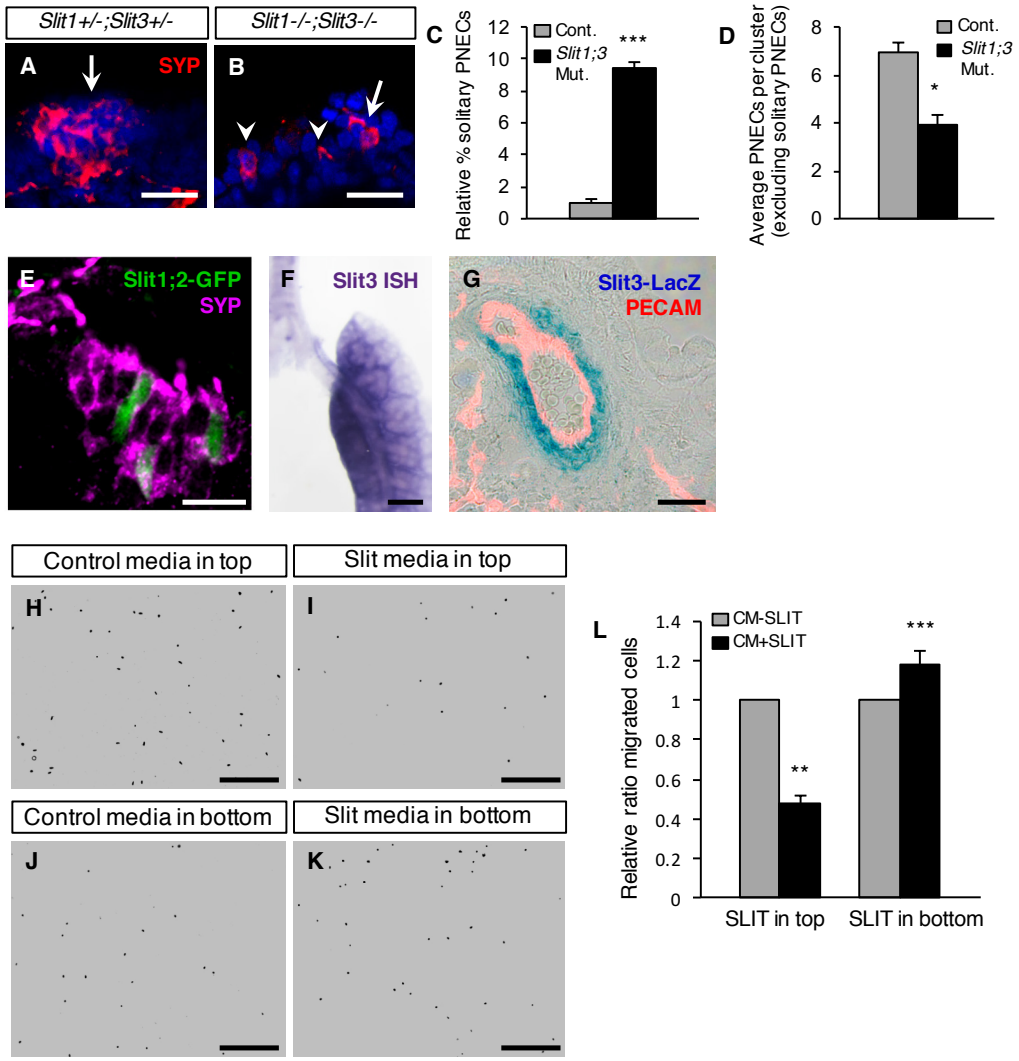

Figure S11. PNEC clustering is a Slit-ligand dependent process.

(A,B) Synaptophysin staining shows clustered (arrows) and solitary (arrowheads) PNECs in P0 lungs. Scale bars, 20 µm. (C) Solitary PNECs are significant increased in *Slit1;3* mutants compared to controls: 9.41% ± 0.38 vs 1% ± 0.23, $p = 1.4x10^{-6}$, n = 4. (D) Number of PNECs per cluster, excluding solitary PNECs, is significantly decreased in *Slit1;3* mutants compared to controls: 3.35 PNECs/cluster ± 0.42 vs 7.33 PNECs/cluster ± 0.48, p = 0.0033, n = 4. (E) *Slit1;2*-GFP is expressed in a subset of PNECs within an NEB outlined by Synaptophysin immunostaining (magenta) at E15.5. Scale bar, 15 µm. (F) *Slit3* expression as detected by RNA in situ hybridization at E13.5. Scale bar, 250 µm. (G) *Slit3*-LacZ, as detected by X-gal staining of β-gal, is observed in pulmonary vascular smooth muscle that surrounds a PECAM-immunostained (red) endothelial vessel at E15.5. Scale bar, 30 µm. (H-K) Representative images of PNECs that migrated from the top to the bottom side of the Boyden chamber are shown by DAPI staining (pseudocolored black). Scale bar, 400 µm. (L) Significantly fewer PNECs

migrated to bottom chamber when cells are cultured with Slit versus control in top chamber: Slit vs control, 0.48 ± 0.04, $p = 8.5x10^{-4}$, n = 5. Significantly more PNECs migrated to bottom chamber when Slit versus control is in bottom chamber: Slit vs control, 1.18 ± 0.07, $p = 7.5x10^{-5}$, n = 5 each. * $p < 0.05$, ** $p < 0.001$, *** $p < 0.0001$. CM = conditioned media.

Branchfield et al.
Figure S12

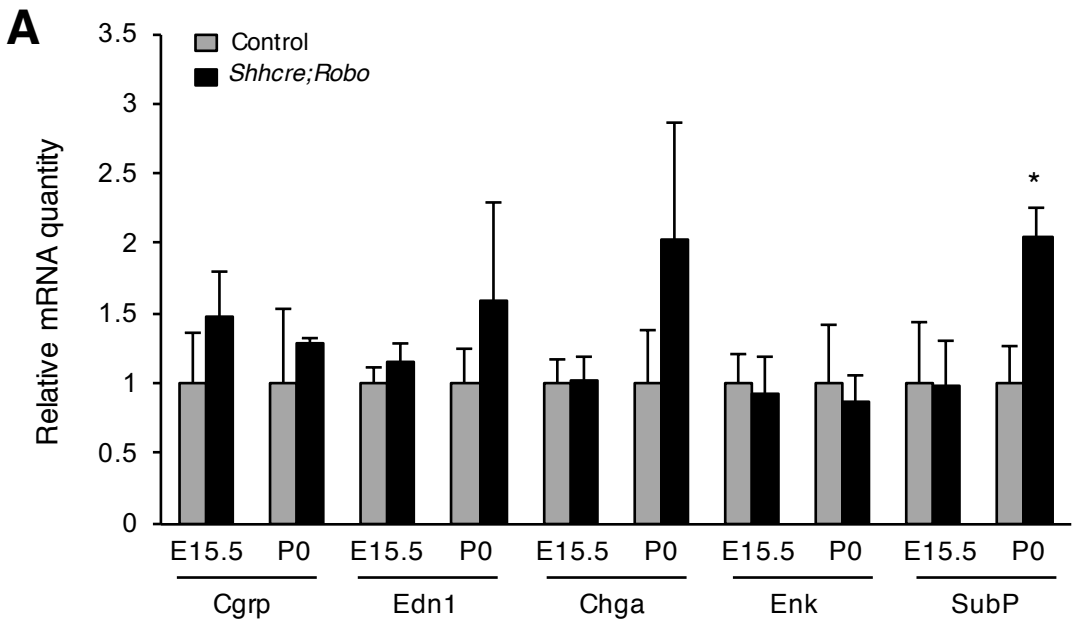

Figure S12. Expression of Substance P, but not other neuropeptide, is upregulated in *Shhcre;Robo* mutant lungs shortly after birth.

(A) qRT-PCR of PNEC neuropeptide genes: calcitonin gene related peptide (Cgrp), endothelin 1 (Edn1), chromogranin A (ChgA), leu-enkephalin (Enk) and substance P (SubP) in *Shhcre;Robo* mutant and control lungs at E15.5 and P0. Substance P transcript levels are increased at P0, but not at E15.5 in *Shhcre;Robo* mutants compared to controls ([E15.5] 0.98 ± 0.32 vs 1 ± 0.43, p = 0.97; [P0] 2.05 ± 0.20 vs 1 ± 0.26, p = 0.03). While expression of other peptides is not significantly altered at these stages (*Shhcre;Robo* mutant vs control: *Cgrp* [E15.5] 1.47 ± 0.32 vs 1 ± 0.37, p = 0.17; *Cgrp* [P0] 1.28 ± 0.04 vs 1 ± 0.53, p = 0.45; *Edn1* [E15.5] 1.16 ± 0.13 vs 1 ± 0.11, p = 0.20; *Edn1* [P0] 1.16 ± 0.13 vs 1 ± 0.11, p = 0.20; *Chga* [E15.5] 1.02 ± 0.16 vs 1 ± 0.17, p = 0.93; *Chga* [P0] 2.01 ± 0.84 vs 1 ± 0.39, p = 0.25; *Enk* [E15.5] 0.93 ± 0.27 vs 1 ± 0.21, p = 0.84; *Enk* [P0] 0.86 ± 0.19 vs 1 ± 0.42, p = 0.77). n = 3 each, * $p < 0.05$.

Branchfield et al.
Figure S13

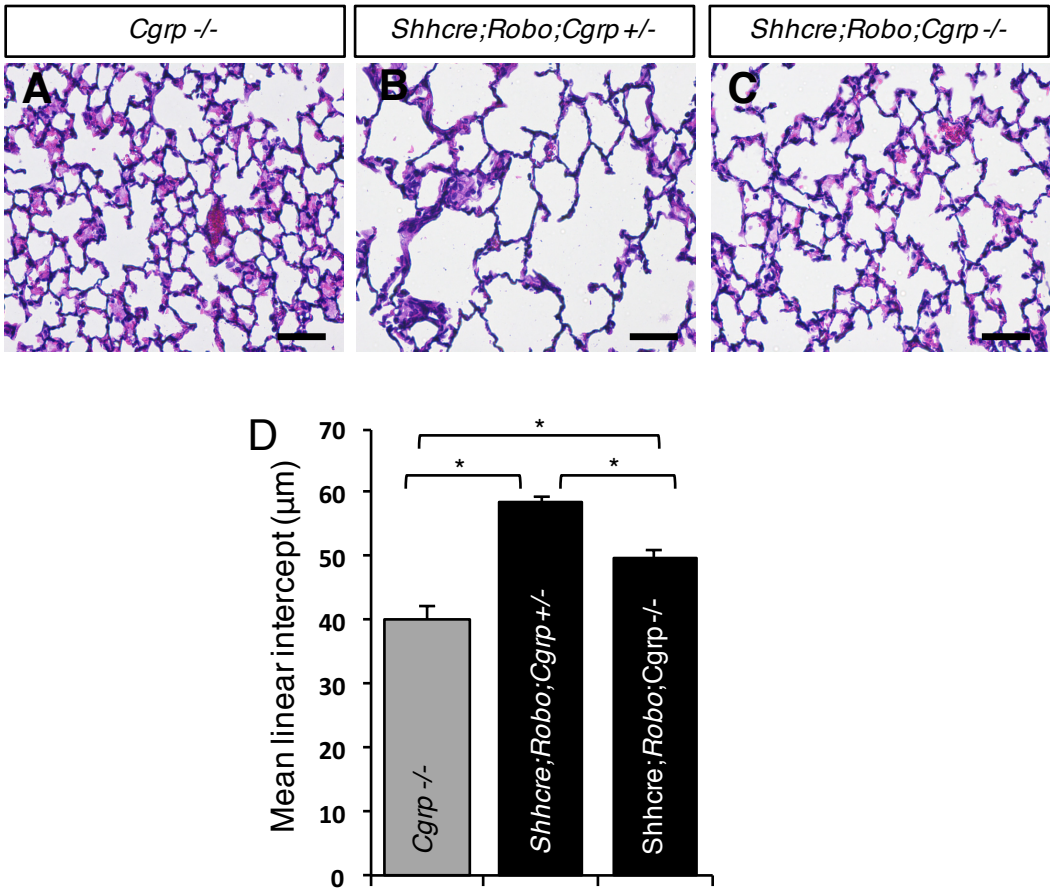

Figure S13. Inactivation of *Cgrp* attenuates alveolar simplification phenotype in *Shhcre;Robo* mutant.

(A-C) H&E staining of alveolar region at P22. Scale bars, 200 µm. (**D**) Quantification of mean linear intercept (MLI): *Cgrp-/-* mutants (40.32µm±2.07), *Shhcre;Robo;Cgrp+/-* mutants (58.47µm ± 1.03), *Shhcre;Robo;Cgrp-/-* mutants (49.86µm ± 1.06). Pair-wise comparisons genotype 1 versus 2, p = 0.0014; genotype 2 versus 3, p = 0.0043; genotype 1 versus 3, p = 0.0148, n = 3 each. *p<0.05, **p<0.01.

Branchfield et al.
Figure S14

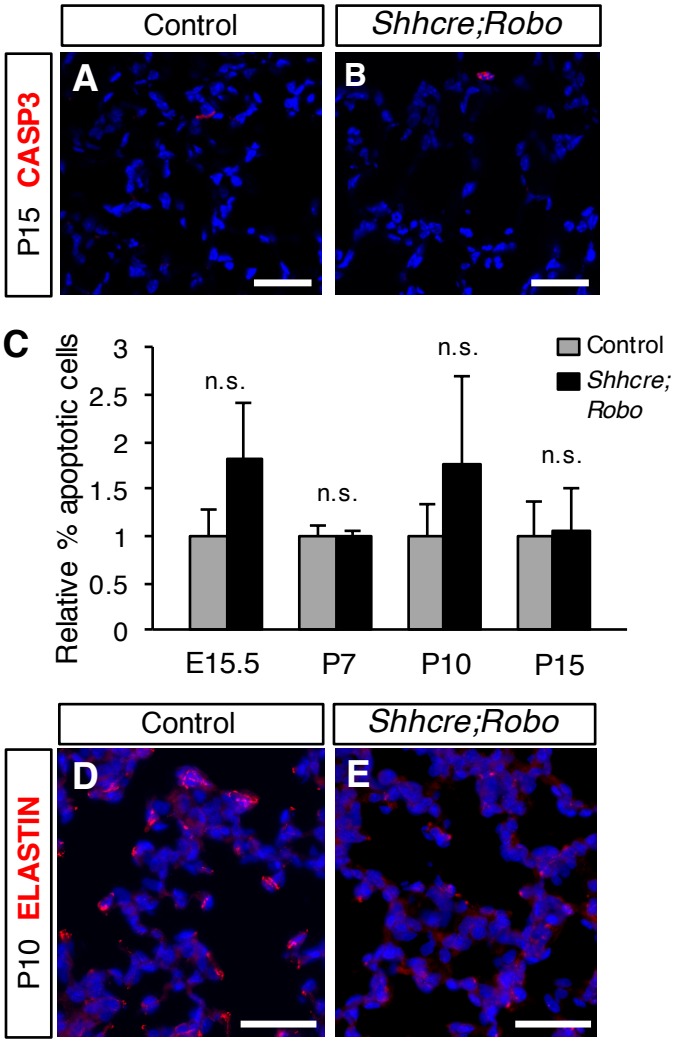

Figure S14. Alveolar simplification is preceded by decreased elastin, but not increased cell death.
(A,B) Cleaved Caspase 3 staining labels apoptotic cells in lungs at P15. (C) Relative percent apoptotic cells in the alveolar region of the lung is not significantly different between the mutant and the control at P15 or earlier stages, n = 6 each. Scale bars, 40 µm. n.s. = not significantly different ($p \geq 0.05$). (D,E) Anti-elastin antibody staining of P10 alveolar region indicating a decrease of staining intensity in the mutant, n=3 each. Scale bars, 50 µm.

Branchfield et al.
Figure S15

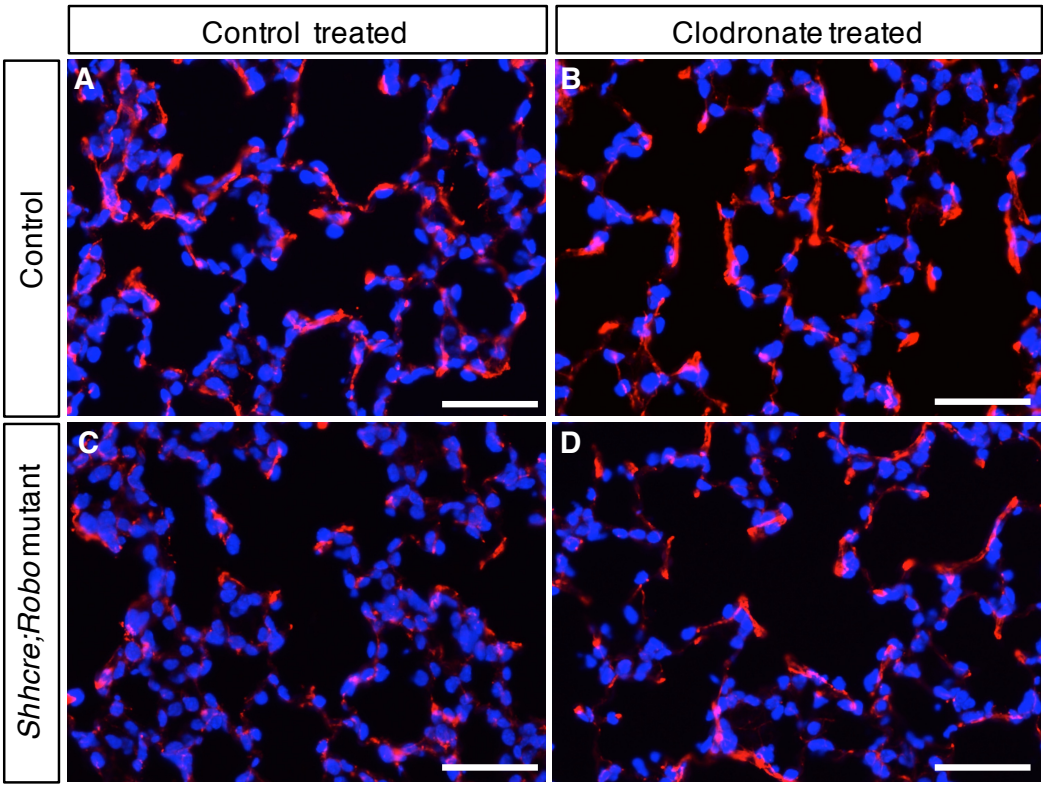

Figure S15. Clodronate treatment attenuates decreased elastin phenotype in *Shhcre;Robo* mutant lungs.

(A-D) P22 alveolar sections stained with anti-Elastin antibody. (A,B) Staining is similar in the alveolar region of control- and clodronate-treated lungs. (C,D) More staining in the clodronate treated versus control treated *Shhcre;Robo* mutants, suggesting partial reversal of Elastin decrease phenotype, n=3 each. Scale bars, 50 μm.

References

1. E. Cutz, J. Pan, H. Yeger, N. J. Domnik, J. T. Fisher, Recent advances and contraversies on the role of pulmonary neuroepithelial bodies as airway sensors. *Semin. Cell Dev. Biol.* **24**, 40–50 (2013). Medline doi:10.1016/j.semcdb.2012.09.003

2. J. E. Boers, J. L. den Brok, J. Koudstaal, J. W. Arends, F. B. Thunnissen, Number and proliferation of neuroendocrine cells in normal human airway epithelium. *Am. J. Respir. Crit. Care Med.* **154**, 758–763 (1996). Medline doi:10.1164/ajrccm.154.3.8810616

3. R. I. Linnoila, Functional facets of the pulmonary neuroendocrine system. *Lab. Invest.* **86**, 425–444 (2006). Medline doi:10.1038/labinvest.3700412

4. H. Song, E. Yao, C. Lin, R. Gacayan, M. H. Chen, P. T. Chuang, Functional characterization of pulmonary neuroendocrine cells in lung development, injury, and tumorigenesis. *Proc. Natl. Acad. Sci. U.S.A.* **109**, 17531–17536 (2012). Medline doi:10.1073/pnas.1207238109

5. E. Cutz, H. Yeger, J. Pan, Pulmonary neuroendocrine cell system in pediatric lung disease-recent advances. *Pediatr. Dev. Pathol.* **10**, 419–435 (2007). Medline doi:10.2350/07-04-0267.1

6. D. G. Perrin, T. J. McDonald, E. Cutz, Hyperplasia of bombesin-immunoreactive pulmonary neuroendocrine cells and neuroepithelial bodies in sudden infant death syndrome. *Pediatr. Pathol.* **11**, 431–447 (1991). Medline doi:10.3109/15513819109064779

7. M. E. Sunday, L. Shan, M. Subramaniam, Immunomodulatory functions of the diffuse neuroendocrine system: Implications for bronchopulmonary dysplasia. *Endocr. Pathol.* **15**, 91–106 (2004). Medline doi:10.1385/EP:15:2:091

8. X. Gu, P. H. Karp, S. L. Brody, R. A. Pierce, M. J. Welsh, M. J. Holtzman, Y. Ben-Shahar, Chemosensory functions for pulmonary neuroendocrine cells. *Am. J. Respir. Cell Mol. Biol.* **50**, 637–646 (2014). Medline doi:10.1165/rcmb.2013-0199OC

9. C. S. Kuo, M. A. Krasnow, Formation of a neurosensory organ by epithelial cell slithering. *Cell* **163**, 394–405 (2015). Medline doi:10.1016/j.cell.2015.09.021

10. S. Tjen-A-Looi, R. Ekman, H. Lippton, J. Cary, I. Keith, CGRP and somatostatin modulate chronic hypoxic pulmonary hypertension. *Am. J. Physiol.* **263**, H681–H690 (1992). Medline

11. S. Dunzendorfer, C. Meierhofer, C. J. Wiedermann, Signaling in neuropeptide-induced migration of human eosinophils. *J. Leukoc. Biol.* **64**, 828–834 (1998). Medline

12. B. D. Moore, D. Hyde, L. Miller, E. Wong, J. Frelinger, E. S. Schelegle, Allergen and ozone exacerbate serotonin-induced increases in airway smooth muscle contraction in a model of childhood asthma. *Respiration* **83**, 529–542 (2012). Medline doi:10.1159/000336835

13. S. Kantarci, P. K. Donahoe, Congenital diaphragmatic hernia (CDH) etiology as revealed by pathway genetics. *Am. J. Med. Genet. C. Semin. Med. Genet.* **145C**, 217–226 (2007). Medline doi:10.1002/ajmg.c.30132

14. M. Longoni, F. A. High, M. K. Russell, A. Kashani, A. A. Tracy, C. M. Coletti, R. Hila, A. Shamia, J. Wells, K. G. Ackerman, J. M. Wilson, C. J. Bult, C. Lee, K. Lage, B. R. Pober, P. K. Donahoe, Molecular pathogenesis of congenital diaphragmatic hernia

revealed by exome sequencing, developmental data, and bioinformatics. *Proc. Natl. Acad. Sci. U.S.A.* **111**, 12450–12455 (2014). Medline doi:10.1073/pnas.1412509111

15. K. S. Harris, Z. Zhang, M. T. McManus, B. D. Harfe, X. Sun, Dicer function is essential for lung epithelium morphogenesis. *Proc. Natl. Acad. Sci. U.S.A.* **103**, 2208–2213 (2006). Medline doi:10.1073/pnas.0510839103

16. E. T. Domyan, K. Branchfield, D. A. Gibson, L. A. Naiche, M. Lewandoski, M. Tessier-Lavigne, L. Ma, X. Sun, Roundabout receptors are critical for foregut separation from the body wall. *Dev. Cell* **24**, 52–63 (2013). Medline doi:10.1016/j.devcel.2012.11.018

17. E. J. Kim, J. L. Ables, L. K. Dickel, A. J. Eisch, J. E. Johnson, Ascl1 (Mash1) defines cells with long-term neurogenic potential in subgranular and subventricular zones in adult mouse brain. *PLOS ONE* **6**, e18472 (2011). Medline

18. B. Hivert, Z. Liu, C. Y. Chuang, P. Doherty, V. Sundaresan, Robo1 and Robo2 are homophilic binding molecules that promote axonal growth. *Mol. Cell. Neurosci.* **21**, 534–545 (2002). Medline doi:10.1006/mcne.2002.1193

19. C. Englund, P. Steneberg, L. Falileeva, N. Xylourgidis, C. Samakovlis, Attractive and repulsive functions of Slit are mediated by different receptors in the *Drosophila* trachea. *Development* **129**, 4941–4951 (2002). Medline

20. E. S. McCoy, B. Taylor-Blake, M. J. Zylka, CGRPα-expressing sensory neurons respond to stimuli that evoke sensations of pain and itch. *PLOS ONE* **7**, e36355 (2012). Medline doi:10.1371/journal.pone.0036355

21. S. I. Mund, M. Stampanoni, J. C. Schittny, Developmental alveolarization of the mouse lung. *Dev. Dyn.* **237**, 2108–2116 (2008). Medline doi:10.1002/dvdy.21633

22. A. Shifren, A. G. Durmowicz, R. H. Knutsen, E. Hirano, R. P. Mecham, Elastin protein levels are a vital modifier affecting normal lung development and susceptibility to emphysema. *Am. J. Physiol. Lung Cell. Mol. Physiol.* **292**, L778–L787 (2007). Medline doi:10.1152/ajplung.00352.2006

23. A. M. Wallace, A. J. Sandford, J. C. English, K. M. Burkett, H. Li, R. J. Finley, N. L. Müller, H. O. Coxson, P. D. Paré, R. T. Abboud, Matrix metalloproteinase expression by human alveolar macrophages in relation to emphysema. *COPD* **5**, 13–23 (2008). Medline doi:10.1080/15412550701817789

24. N. van Rooijen, E. Hendrikx, Liposomes for specific depletion of macrophages from organs and tissues. *Methods Mol. Biol.* **605**, 189–203 (2010). Medline doi:10.1007/978-1-60327-360-2_13

25. L. Ma, M. Tessier-Lavigne, Dual branch-promoting and branch-repelling actions of Slit/Robo signaling on peripheral and central branches of developing sensory axons. *J. Neurosci.* **27**, 6843–6851 (2007). Medline doi:10.1523/JNEUROSCI.1479-07.2007

26. A. S. Plump, L. Erskine, C. Sabatier, K. Brose, C. J. Epstein, C. S. Goodman, C. A. Mason, M. Tessier-Lavigne, Slit1 and Slit2 cooperate to prevent premature midline crossing of retinal axons in the mouse visual system. *Neuron* **33**, 219–232 (2002). Medline doi:10.1016/S0896-6273(01)00586-4

27. W. Yuan, Y. Rao, R. P. Babiuk, J. J. Greer, J. Y. Wu, D. M. Ornitz, A genetic model for a central (septum transversum) congenital diaphragmatic hernia in mice lacking Slit3. *Proc. Natl. Acad. Sci. U.S.A.* **100**, 5217–5222 (2003). Medline doi:10.1073/pnas.0730709100

28. K. Schnorbusch, R. Lembrechts, I. Pintelon, J. P. Timmermans, I. Brouns, D. Adriaensen, GABAergic signaling in the pulmonary neuroepithelial body microenvironment: Functional imaging in GAD67-GFP mice. *Histochem. Cell Biol.* **140**, 549–566 (2013). Medline doi:10.1007/s00418-013-1093-x